NeuroImage: Clinical 13 (2017) 97–105

Contents lists available at ScienceDirect

NeuroImage: Clinical

journal homepage: www.elsevier.com/locate/ynicl

CAG repeat length does not associate with the rate of cerebellar degeneration in spinocerebellar ataxia type 3

Shang-Ran Huang[a,1], Yu-Te Wu[a,b,1], Chii-Wen Jao[b], Bing-Wen Soong[c,d], Jiing-Feng Lirng[d,e], Hsiu-Mei Wu[d,e], Po-Shan Wang[b,c,d,f,*]

[a]Department of Biomedical Imaging and Radiological Sciences, National Yang-Ming University, No.155, Sec. 2, Linong St., Taipei, Taiwan
[b]Institute of Biophotonics, National Yang-Ming University, No.155, Sec. 2, Linong St., Taipei, Taiwan
[c]Department of Neurology, Neurological Institute, Taipei Veterans General Hospital, No.201, Sec. 2, Shipai Rd., Taipei, Taiwan
[d]School of Medicine, National Yang-Ming University, No.155, Sec. 2, Linong St., Taipei, Taiwan
[e]Department of Radiology, Taipei Veterans General Hospital, No.201, Sec. 2, Shipai Rd., Taipei, Taiwan
[f]Department of Neurology, Taipei Municipal Gan-Dau Hospital, No.12, Ln. 225, Zhixing Rd., Taipei, Taiwan

ARTICLE INFO

Article history:
Received 30 August 2016
Received in revised form 7 November 2016
Accepted 9 November 2016
Available online 10 November 2016

Keywords:
Brain connectivity
Fractal dimension
Magnetic resonance imaging
Magnetic resonance spectroscopy
NAA
SCA3

ABSTRACT

This cross-sectional study investigated the correlation between the CAG repeat length and the degeneration of cerebellum in spinocerebellar ataxia type 3 (SCA3) patients based on neuroimaging approaches. Forty SCA3 patients were recruited and classified into two subgroups according to their CAG repeat lengths (≥74 and <74). We measured each patient's Scale for the Assessment and Rating of Ataxia (SARA) score, *N*-acetylaspartate (NAA)/creatine (Cr) ratios based on magnetic resonance spectroscopy (MRS), and 3-dimensional fractal dimension (3D-FD) values derived from magnetic resonance imaging (MRI) results. Furthermore, the 3D-FD values were used to construct structural covariance networks based on graph theoretical analysis. The results revealed that SCA3 patients with a longer CAG repeat length demonstrated earlier disease onset. However, the CAG repeat length did not significantly correlate with their SARA scores, cerebellar NAA/Cr ratios or cerebellar 3D-FD values. Network dissociation between cerebellar regions and parietal-occipital regions was found in SCA3 patients with CAG ≥ 74, but not in those with CAG < 74. In conclusion, the CAG repeat length is uncorrelated with the change of SARA score, cerebellar function and cerebellar structure in SCA3. Nevertheless, a longer CAG repeat length may indicate early structural covariance network dissociation.

1. Introduction

Spinocerebellar ataxia type 3 (SCA3), also referred to as Machado–Joseph disease, is an autosomal dominant neurodegenerative disorder (do Carmo Costa and Paulson, 2012). Progressive ataxia, external ophthalmoplegia, dysarthria, dysphagia, pyramidal signs, dystonia, and rigidity are common clinical features of SCA3 (do Carmo Costa and Paulson, 2012), and some patients also manifest extracerebellar pathologies, such as spinal cord affections, peripheral polyneuropathy and basal ganglia disease (Pedroso et al., 2013). The cerebellum is one of the well-known regions mainly affected in SCA3 patients. Especially, cerebellar nuclei are primarily affected at the beginning of the disease. Many neuropathology studies (Durr et al., 1996; Koeppen, 2005; Scherzed et al., 2012; Takiyama et al., 1994) have reported atrophy or neuronal loss in the cerebellar cortex, vermis, peduncles, and deep nuclei. Structural or functional degeneration of the cerebellum can be observed by different neuroimaging approaches including magnetic resonance imaging (MRI) volumetry (Eichler et al., 2011; Klockgether et al., 1998b; Reetz et al., 2013; Schulz et al., 2010; Stefanescu et al., 2015), diffusion tensor imaging (DTI) (Guimaraes et al., 2013), magnetic resonance spectroscopy (MRS) (Adanyeguh et al., 2015; Lirng et al., 2012; Wang et al., 2012), and position emission tomography (Wang et al., 2007).

Some studies have reported that SCA3 may be caused by abnormal CAG repeat expansion in the coding region of chromosome 14q32.1 (Kawaguchi et al., 1994; Takiyama et al., 1994). The CAG repeat length substantially affects the clinical characteristics of SCA3 patients (do Carmo Costa and Paulson, 2012). For example, in healthy subjects, the CAG repeat length in the gene should be shorter than 44; a CAG repeat length longer than 60 may lead to the manifestation of clinical symptoms in SCA3 patients (do Carmo Costa and Paulson, 2012). Moreover, SCA3 patients with a longer CAG repeat length may exhibit more rapid progression through disease stages (Klockgether et al., 1998a). The CAG repeat length is also negatively correlated with the age of onset (AO) of SCA3 patients (Durr et al., 1996; Maciel et al., 1995).

* Corresponding author at: Department of Neurology, Taipei Municipal Gan-Dau Hospital, No.12, Ln. 225, Zhixing Rd., Taipei, Taiwan.
E-mail address: b8001071@gmail.com (P.-S. Wang).
[1] The authors contributed equally to this article.

http://dx.doi.org/10.1016/j.nicl.2016.11.007

Therefore, SCA3 patients with a longer CAG repeat length are considered to possibly exhibit more rapid disease progression, subsequently leading to earlier disease onset. A more rapid disease progression can partly, if not wholly, be ascribed to more rapid cerebellar degeneration, because the cerebellum is the major disease-involved region in SCA3. To date, it has been speculated that there is a correlation between the CAG repeat length and the cerebellar degeneration of SCA3 patients. However, reports with positive and negative evidence make the inference inconclusive (D'Abreu et al., 2012; Eichler et al., 2011; Klockgether et al., 1998b; Onodera et al., 1998; Reetz et al., 2013; Schulz et al., 2010; Stefanescu et al., 2015).

This study comprehensively investigated the mechanisms by which the CAG repeat length influences the cerebellar degeneration of SCA3 patients from 3 different perspectives, namely cerebellar function, cerebellar structure, and cerebellar structural network based on MRS and MRI. The *N*-acetylaspartate (NAA) concentration is considered an indicator of neuronal integrity (Bachelard and Badar-Goffer, 1993). Therefore, the NAA concentration measured by MRS can serve as a functional probe for cerebellar dysfunction. Our previous study (Wang et al., 2012) has reported that the ratios of NAA to creatine (Cr) in the right cerebellum (Rt-Cb-NAA), left cerebellum (Lt-Cb-NAA), and vermis (V-NAA) were significantly lower in SCA3 patients than in controls, and these ratios were closely correlated with the score of Scale for the assessment and rating of ataxia (SARA) (Schmitz-Hübsch et al., 2006). In contrast to the NAA measurement, the three-dimensional fractal dimension (3D-FD) method is an efficient quantifier for cortical folding complexity assessment, and 3D-FD is effective for studying the morphological change in the cortical structure caused by various neurological disorders based on MRI images (Ha et al., 2005; King et al., 2010; Sandu et al., 2008; Thompson et al., 2005). Our previous studies have applied this method to detect brain atrophy in multiple system atrophy of the cerebellar type (Wu et al., 2010) and SCA3 (Wang et al., 2015).

Complementary to measuring the impairment of the cerebellar function and structure based on the NAA and 3D–FD, graphic-based brain network analysis can be used to analyse the destruction or reorganisation of brain networks caused by neurological diseases (Braun et al., 2009; Rubinov and Sporns, 2010). The brain network is constructed by a collection of nodes and links, in which the nodes represent brain regions and the links represent connections between paired brain regions. These connections can be structural, functional, or effective depending on the type of data set (Friston, 1994). Recently, many studies (Alexander-Bloch et al., 2013; Evans, 2013) have investigated brain networks constructed based on the structural covariance between brain regions across a group of subjects. Such structural covariance networks showed similarity with the results of DTI tractography (Gong et al., 2012; Lerch et al., 2006) and functional MRI (fMRI) (Wang et al., 2014). These results provided the motivational basis for us to use the morphometric index of 3D-FD to establish the structural brain network of SCA3 patients.

In this study, we hypothesised that the CAG repeat length is correlated with the change of cerebellar function and structure in SCA3. We used NAA/Cr ratios and 3D-FD values to investigate the influence of the CAG repeat length on the cerebellar function and structure of SCA3 patients. Furthermore, graphic-based brain network analysis was performed to determine whether the CAG repeat length affects the network between the cerebellum and other brain regions.

2. Materials and methods

2.1. Patients and controls

This study was approved by the Institutional Review Board of Taipei Veterans General Hospital, Taipei, Taiwan and carried out in accordance with The Code of Ethics of the World Medical Association (Declaration of Helsinki). Informed consent was obtained from each participant before commencement of this study. Forty SCA3 patients were recruited for this study. Another 80 age- and sex-matched healthy subjects (40 for the MRS study and 40 for the MRI study) were recruited as the control groups. All SCA3 patients were evaluated by SARA. SARA score (Schmitz-Hübsch et al., 2006), which was a rating of the severity of ataxia symptoms ranging from 0 to 40, was used as a reference to indicate the progression of clinical severity in comparison with the cerebellar degeneration. A self-reported AO was acquired from each patient. The AO was defined as the age at which the patients showed the first sign of any ataxic symptom (Jardim et al., 2001). Disease duration was calculated accordingly. Hereafter, capitalised Age and Duration represent the participants' age at the date of examination and the corresponding disease duration (Duration is only available for the SCA3 patients), respectively. The CAG repeat length of each SCA3 patient was determined by polymerase chain reaction, as described previously (Soong et al., 2001). Disease duration-adjusted SARA scores (SARA/Duration) of the SCA3 patients were computed. To explore the possible nonlinear nature of the disease progression pattern of SCA3, we divided the SCA3 patients into two subgroups according to a CAG repeat length threshold of 74 (≥ 74 and <74). This criterion is based on the mean CAG repeat length (73.2 ± 4.0) of the SCA3 patients, and it can generate more balanced sample sizes (22 vs 18) for the two subgroups. We confirmed that the control groups did not exhibit any central nervous disease or neurological abnormalities before or during the study period. In addition, the T1- and T2-weighted images of the control groups were examined to ensure the absence of latent neurological diseases or unexpected abnormalities.

2.2. Image acquisition

Brain MRI and MRS images were obtained using a 1.5-T system (Signa EXCITE, GE Medical Systems, Milwaukee, WI, USA). The MRI protocol involved an axial, T1-weighted, 3-dimensional, fast-spoiled, gradient-recalled acquisition of steady state images (TR [repetition time] = 8.58 ms, TE [echo time] = 3.62 ms, inversion time [TI] = 400 ms, slice thickness = 1.5 mm) and an axial, T2-weighted, fast spin-echo sequence (TR = 4000 ms, TE = 256.5 ms, slice thickness = 5 mm). After MRI images were acquired, proton MRS was performed with a single-voxel, stimulated echo-acquisition mode sequence (TR/TE/mixing time/excitations = 3000/15/13.7/96, spectral width = 2500 Hz, number of points = 2048, voxel size = 2 cm × 2 cm × 2 cm) in the regions of the bilateral cerebellar hemispheres and the cerebellar vermis of subjects. For each subject, the selection of the voxel of interest (VOI) was performed by the same investigator to ensure consistent placement. The locations of these VOIs were confirmed to be accurate by 2 other investigators by overlaying the 3-dimensional maps on the corresponding T2-weighted images. The precise locations of VOIs were described in our previous study (Wang et al., 2012). The NAA and Cr measurements were derived by software implemented in MRI equipment. Care was taken to avoid the inclusion of cerebrospinal fluid-filled spaces within the VOIs. Peak areas for NAA at 2.02 parts per million (ppm) and creatine (Cr) at 3.03 ppm were calculated using FuncTool software (GE Healthcare, Milwaukee, WI, USA). Peak integral values were expressed relative to the Cr peak. Three NAA/Cr ratios, namely Rt-Cb-NAA, Lt-Cb-NAA, and V-NAA, were calculated. To ensure high-quality images, MRS results with a full width at half maxima >6 Hz were disqualified from the MRS analysis. According to this criterion, the value of Rt-Cb-NAA in one subject, those of Lt-Cb-NAA in 2 subjects, and those of V-NAA in 3 subjects were removed. Two values of V-NAA in the controls were also unavailable.

2.3. 3D-FD value computation

FD analysis was originally proposed to quantify the shape complexity of objects into a simple numerical value. Preprocessing was performed before the computation of 3D-FD values according to T1-weighted MRI results. The preprocessing procedures are illustrated in

the flowchart in Fig. 1. The acquired T1-weighted image was first resampled to 1 × 1 × 1 mm by using ImageJ (Rasband WS, ImageJ, U. S. National Institutes of Health, Bethesda, Maryland, USA, http://imagej.nih.gov/ij/, 1997–2016) (Fig. 1(a)). Before the segmentation of brain tissue, an automated skull-stripping function was applied to the image volumes by using the brain extraction tool in MRIcro software (Rorden C, University of Nottingham, UK; www.sph.sc.edu/comd/rorden/mricro.html) (Fig. 1(b)). The skull-stripped images were then normalised to the JHU_MNI_SS_T_ss T1 template by a 12-parameter affine transformation in the DiffeoMap toolbox (Li X, Jiang H, and Mori S, Johns Hopkins University, www.MriStudio.org) (Fig. 1(c)). Brain segmentation was performed using the SPM8 toolbox (Welcome Department of Cognitive Neurology, Institute of Neurology, University College London, London, UK, http://www.fil.ion.ucl.ac.uk/spm/) (Fig. 1(d)). Brain region labelling was performed according to Individual Brain Atlases using Statistical Parametric Mapping (IBASPM) (http://www.thomaskoenig.ch/Lester/ibaspm.htm) toolbox in MATLAB R2013b software (Mathworks, Natick, MA, USA). The brain cortex was subsequently parcellated into 116 separate regions by using the Automated Anatomical Labelling (AAL) atlas based on IBASPM (Fig. 1(e)). The 26 regions of the cerebellum were then merged into 7 regions, namely the left anterior lobe, right anterior lobe, left posterior upper lobe, right posterior upper lobe, left posterior lower lobe, right posterior lower lobe, and vermis, according to their anatomical structures. Hence, 97 labelled brain regions were obtained for each subject (Fig. 1(f)).

In this study, we adopted the 3D box-counting method to calculate the 3D-FD values of the 97 labelled brain regions for each subject. The box-counting algorithm has been explained in our previous study (Wu et al., 2010).

2.4. Brain network analysis

To investigate whether different CAG repeat lengths cause a difference in the brain network of SCA3 patients, the patients whose disease duration is not ≤5 years were excluded in each SCA3 subgroup for the following brain network analysis. This criterion of disease duration ≤5 years was selected to minimise the effect of disease duration, to ensure that the data were representative of the network status close to the AO. Moreover, the criterion ensured an adequate number of subjects in each SCA3 subgroup as required for the brain network analysis. After the exclusion of SCA3 patients who did not meet the criterion, 8 and 7 subjects were included in the subgroups with CAG < 74 and CAG ≥ 74, respectively. Accordingly, 2 new control groups age- and sex-matched to their corresponding SCA3 counterparts were formed, and they were denoted by Control I and Control II. No healthy subject was repeatedly selected into the 2 control groups.

After obtaining the 3D-FD values of 97 brain regions, we computed the region-to-region correlations based on the derived 3D-FD values and formed a 97 × 97 correlation matrix for each group. Subsequently, the values in the correlation matrix with a p-value of <0.05 were set to 1, and the remaining values in other entries were set to 0. This binarised correlation matrix is called an adjacency matrix in graph theory, in which 1 implies the presence of a link between 2 corresponding brain regions (nodes) and 0 implies the absence of a link. Subsequently, diagrams were created to illustrate the architecture of the cerebellar networks on a glass brain template.

2.5. Statistical analyses

All data are expressed as mean ± standard deviation ($\bar{x} \pm s$). Outliers of NAA/Cr ratios and 3D-FD values outside the range of mean ± 2 × standard deviation were removed in the subsequent analysis. Parameters between the patients and controls, between the two patients subgroups, and between the patients subgroups and controls were all compared using the 2-sample t-test. The sex ratios were compared using the Pearson chi-squared test. The Pearson correlation and a scatter plot (Fig. 2) were used to display the relation between the CAG repeat length and AO. The Pearson correlation between CAG repeat length and SARA score/Duration was computed. A multivariate linear regression analysis was used to investigate how independent variables (predictors), namely the AO, Duration, CAG repeat length, and the interaction term (AO:CAG), accounted for the variance of dependent variables, namely SARA score, NAA/Cr ratios and 3D-FD values. A false discovery rate (FDR) controlling procedure (Benjamini and Hochberg, 1995) was applied to reduce type I error caused by multiple comparisons in the regression model.

Scatter plots of the SARA score versus Duration (Fig. 3), NAA/Cr ratios versus Duration (Fig. 4), and 3D-FD values versus Duration (Fig. 5) were constructed to illustrate the degeneration patterns of the SARA score, NAA/Cr ratios, and 3D-FD values, respectively, in the SCA3

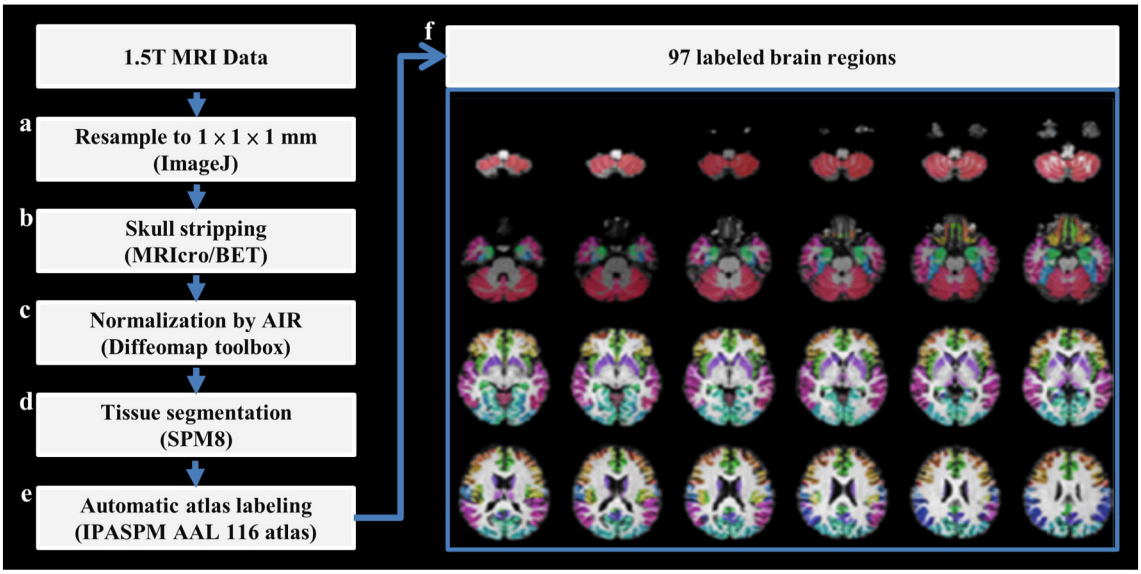

Fig. 1. Flowchart of image preprocessing. Each voxel of grey matter in the T1-weighted image was labelled according to the 116 regions of the AAL atlas. Subsequently, the 26 cerebellar regions were merged into 7 cerebellar regions based on anatomical position, resulting in the final 97 labelled brain regions, which are displayed in different colours in the right panel. (For interpretation of the references to colour in this figure legend, the reader is referred to the web version of this article.)

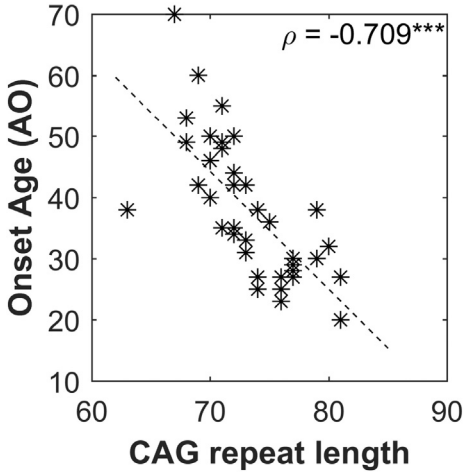

Fig. 2. Graph of CAG repeat length versus onset age (AO).

subgroups. The parallelism levels of the slopes of the SARA score versus Duration, NAA/Cr ratios versus Duration, and 3D-FD values versus Duration between the SCA3 subgroups were tested using a linear regression model.

3. Results

3.1. Cerebellar NAA/Cr ratios and 3D-FD values were lower in the SCA3 patients

The detailed demographic data, clinical data, NAA values, and 3D-FD values of the participants are summarised in Table 1. The results of neurological examination for extracerebellar symptoms were added into the Appendix A. Supplementary data. No difference in age was observed between the SCA3 patients and the MRS control group (45.9 ± 11.9 vs 51.20 ± 17.58, $p = 0.114$) or the MRI control group (45.9 ± 11.9 vs 43.5 ± 11.2, $p = 0.377$). The SCA3 patients showed significantly lower NAA/Cr ratios than did the controls (all $p < 0.001$) in the right cerebellum, left cerebellum, and vermis, and these ratios are respectively outlined as follows: Rt-Cb-NAA, 0.82 ± 0.15 versus 1.00 ± 0.11; Lt-Cb-NAA, 0.85 ± 0.15 versus 1.00 ± 0.13; and V-NAA, 0.78 ± 0.10 versus 0.90 ± 0.11. Similarly, the SCA3 patients showed significantly lower 3D-FD values than did the controls in the right anterior lobe (2.02 ± 0.08 vs 2.10 ± 0.04, $p < 0.001$), left anterior lobe (2.08 ± 0.08 vs 2.12 ± 0.04, $p < 0.01$), right posterior upper lobe (2.41 ± 0.04 vs 2.43 ± 0.02, $p < 0.05$), left posterior lower lobe (2.32 ± 0.06 vs 2.34 ± 0.04, $p < 0.05$), and whole cerebellum (2.48 ± 0.04 vs 2.51 ± 0.02, $p < 0.001$).

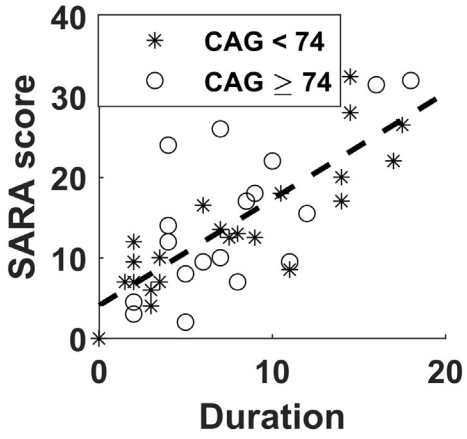

Fig. 3. Graph of SARA score versus Duration. Stars represent the subgroup with CAG < 74, and circles represent the subgroup with CAG ≥ 74. The dash line represents the common slope of the SCA3 subgroups.

3.2. SCA3 patients with a longer CAG repeat length demonstrated earlier disease onset

Overall, the data of the recruited SCA3 patients revealed a negative correlation between the CAG repeat length and AO ($\rho = -0.709$, $p < 0.001$). The scatter plot of CAG repeat length versus AO was displayed in Fig. 2.

3.3. CAG repeat length was not correlated with SARA score/Duration

The result showed that the CAG repeat length was not correlated with SARA score/Duration ($\rho = -0.059$, $p = 0.720$). No difference was observed in SARA score/Duration between the SCA3 subgroup with CAG < 74 and the subgroup with CAG ≥ 74 (2.3 ± 1.4 vs 2.1 ± 1.3, $p = 0.634$) (Table 1).

3.4. CAG repeat length was not a significant determinant of SARA score, NAA/Cr ratios, and 3D-FD values

The results of multivariate linear regression are summarised in Table 2. The values in Table 2 represent the estimated coefficient of the predictors. The results showed that Duration was significantly correlated with SARA score and all 3 cerebellar NAA/Cr ratios. However, Duration was not correlated with any 3D-FD value. Besides, AO and the CAG repeat length were not correlated with SARA score, NAA/Cr ratios and 3D-FD values.

Similarly, analysing the SCA3 subgroups separately revealed that the CAG repeat length was not a significant determinant of SARA score, any NAA/Cr ratio or 3D-FD value. The regression results for the two SCA3 subgroups are presented in the Appendix A. Supplementary data.

3.5. No difference in slopes of SARA score, NAA/Cr ratios, and 3D-FD values versus Duration between the two SCA3 subgroups

Scatter plots of the SARA score, NAA/Cr ratios, and 3D-FD values versus Duration are displayed in Figs. 3, 4, and 5, respectively. In these plots, stars represent the SCA3 patients with CAG < 74 and circles represent the SCA3 patients with CAG ≥ 74. Instead of drawing individual slopes for each SCA3 subgroup, we drew only the common slope of the 2 subgroups to accentuate the fact that no significant difference was observed in the degeneration rate of these parameters versus Duration.

The scatter plot of the SARA score versus Duration is shown in Fig. 3. No significant difference was observed in the slopes of SARA scores versus Duration between the two SCA3 subgroups ($F = 0.37$, $p = 0.549$). The scatter plots of Rt-Cb-NAA, Lt-Cb-NAA, and V-NAA versus Duration are displayed in Fig. 4(a), (b), and (c), respectively. The tests of slope parallelism revealed no difference in Rt-Cb-NAA versus Duration ($F = 1.15$, $p = 0.291$), Lt-Cb-NAA versus Duration ($F = 0.04$, $p = 0.847$), and V-NAA versus Duration ($F = 0.67$, $p = 0.419$) between the SCA3 subgroups. The scatter plots of FD values in the left anterior lobe (Lt-A-FD), right anterior lobe (Rt-A-FD), left posterior upper lobe (Lt-PU-FD), right posterior upper lobe (Rt-PU-FD), left posterior lower lobe (Lt-PL-FD), right posterior lower lobe (Rt-PL-FD), and whole volume (Cb-FD) of the cerebellum versus Duration are displayed in Fig. 5(a), (b), (c), (d), (e), (g), and (h), respectively. No significant difference was observed in the slopes of Lt-A-FD versus Duration ($F = 1.19$, $p = 0.283$), Rt-A-FD versus Duration ($F = 0.34$, $p = 0.564$), Lt-PU-FD versus Duration ($F = 0$, $p = 0.987$), Rt-PU-FD versus Duration ($F = 0.32$, $p = 0.577$), Lt-PL-FD versus Duration ($F = 0.14$, $p = 0.707$), Rt-PL-FD versus Duration ($F = 1.26$, $p = 0.269$), V-FD versus Duration ($F = 0.18$, $p = 0.678$), and Cb-FD versus Duration ($F = 0.63$, $p = 0.434$) between the SCA3 subgroups.

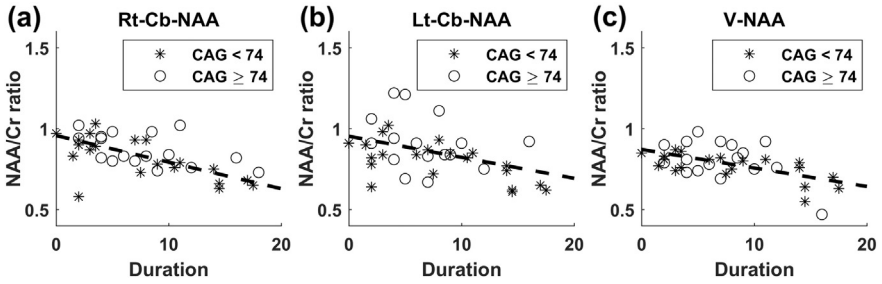

Fig. 4. Graphs of NAA/Cr ratios versus Duration. (a) Rt-Cb-NAA versus Duration, (b) Lt-Cb-NAA versus Duration, and (c) V-NAA versus Duration. Stars represent the subgroup with CAG < 74, and circles represent the subgroup with CAG ≥ 74. The dash lines represent the common slopes of the SCA3 subgroups.

3.6. Network dissociation was found in the SCA3 subgroup with CAG ≥ 74

The demographic and clinical data used in the network analysis are presented in Table 3. The SCA3 subgroups with CAG < 74 and CAG ≥ 74 comprised 8 subjects (M/F = 5/3) and 7 subjects (M/F = 6/1), respectively. A significant difference was observed in Age (50.5 ± 10.6 vs 32.4 ± 5.9, $p < 0.001$), the AO (48.1 ± 11.2 vs 28.7 ± 5.9, $p < 0.01$), and the CAG repeat length (69.0 ± 3.0 vs 76.0 ± 2.4, $p < 0.001$) between the SCA3 subgroups. By contrast, no significant difference was observed in Duration (2.4 ± 1.2 vs 3.7 ± 1.3, $p = 0.051$), SARA score (6.9 ± 3.8 vs 9.6 ± 7.8, $p = 0.396$), and SARA score/Duration (3.2 ± 1.7 vs 2.6 ± 1.8, $p = 0.533$) between the two SCA3 subgroups.

The numbers of total links in the structural covariance networks were 444 in Control I, 385 in Control II, 355 in the SCA3 subgroup with CAG < 74, and 259 in the SCA3 subgroup with CAG ≥ 74. The brain networks of the controls and SCA3 patients are illustrated in Fig. 6(a)–(d), in which only cerebellum-associated links and nodes are plotted. The nodes in the same brain region are coded in the same colour (refer to the figure caption for details). The links are colour coded depending on which corresponding nodes (frontal, parietal, temporal, etc.) are connected to the cerebellar nodes (refer to the figure caption for details).

The cerebellar networks in Controls I and II displayed many links between the cerebellar nodes and the nodes in the frontal (red), parietal (green), temporal (yellow), occipital (blue), and other regions (Fig. 6(a) and (b)). Specifically considering the parietal-occipital lobes (green-blue) revealed that of the 28 parietal-occipital regions in 116 regions of the AAL atlas, 11 regions (approximately 39.3%) in Control I and 14 regions (approximately 50.0%) in Control II were connected to the cerebellar regions (Fig. 6(a) and (b)). A similar connection pattern was observed in the SCA3 subgroup with CAG < 74, in which 6 (6/28, approximately 21.4%) parietal-occipital regions were connected to the cerebellar regions (Fig. 6(c)). However, a marked dissociation of the brain network between the parietal-occipital regions and cerebellar regions was found for the subgroup with CAG ≥ 74, in which only 2 (2/28, approximately 7.1%) parietal-occipital regions were connected to the cerebellar regions (Fig. 6(d)).

4. Discussion

4.1. NAA/Cr ratios and 3D-FD values can indicate cerebellar degeneration in SCA3

According to Table 1, Rt-Cb-NAA, Lt-Cb-NAA, V-NAA, Lt-A-FD, Rt-A-FD, Rt-PU-FD, Lt-PL-FD, and Cb-FD were significantly lower in the SCA3

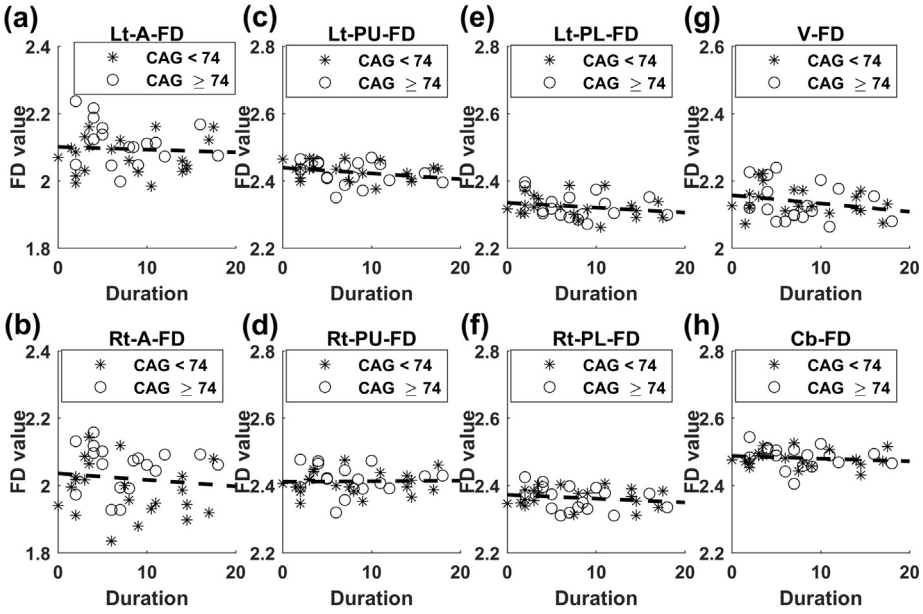

Fig. 5. Graphs of 3D-FD values versus Duration. (a) Lt-A-FD versus Duration, (b) Rt-A-FD versus Duration, (c) Lt-PU-FD versus Duration, (d) Rt-PU-FD versus Duration, (e) Lt-PL-FD versus Duration, (f) Rt-PL-FD versus Duration, (g) V-FD versus Duration, and (h) Cb-FD versus Duration. Stars represent the subgroup with CAG < 74, and circles represent the subgroup with CAG ≥ 74. The dash lines represent the common slopes of the SCA3 subgroups. Lt-A-FD: left anterior lobe FD, Rt-A-FD: right anterior lobe FD, Lt-PU-FD: left posterior upper lobe FD, Rt-PU-FD: right posterior upper lobe FD, Lt-PL-FD: left posterior lobe FD, Rt-PL-FD: right posterior lobe FD, V-FD: vermis FD, Cb-FD: FD of the whole cerebellum.

Table 1
Demographic data, clinical data, MRS NAA measurements, and MRI 3D-FD measurements derived from controls and SCA3 patients.

Variables	Control ($n = 40$)	SCA3 ($n = 40$)	SCA3	SCA3	p-Value
			CAG < 74 ($n = 22$)	CAG ≥ 74 ($n = 18$)	
Age of onset (AO) (year)	ND	38.1 ± 10.9	44.9 ± 9.5	29.9 ± 5.6	<0.001***
Duration (year)	ND	7.7 ± 5.0	7.8 ± 5.6	7.7 ± 4.4	0.962
SARA	ND	14.2 ± 8.6	13.8 ± 8.2	14.8 ± 9.3	0.725
CAG repeat length	ND	73.2 ± 4.0	70.3 ± 2.4	76.7 ± 2.4	<0.001***
SARA/Duration (year)	ND	2.2 ± 1.3	2.3 ± 1.4	2.1 ± 1.3	0.634
MRS study:					
Age (year)	51.20 ± 17.58	45.9 ± 11.9	52.7 ± 10.8	37.6 ± 6.9††	<0.001***
M/F	20/20	20/20	10/12	10/8	0.526[a]
Rt-Cb-NAA	1.00 ± 0.11	0.82 ± 0.15†††	0.79 ± 0.17†††	0.85 ± 0.12†††	0.172
Lt-Cb-NAA	1.00 ± 0.13	0.85 ± 0.15†††	0.81 ± 0.13†††	0.91 ± 0.16†	0.043*
V-NAA	0.90 ± 0.11	0.78 ± 0.10†††	0.76 ± 0.08†††	0.81 ± 0.12††	0.196
MRI study:					
Age (year)	43.5 ± 11.2	45.9 ± 11.9	52.7 ± 10.8††	37.6 ± 6.9†	<0.001***
M/F	20/20	20/20	10/12	10/8	0.526[a]
Lt-A-FD	2.12 ± 0.04	2.08 ± 0.08††	2.07 ± 0.07†††	2.10 ± 0.08	0.168
Rt-A-FD	2.10 ± 0.04	2.02 ± 0.08†††	1.99 ± 0.08†††	2.05 ± 0.07††	0.007**
Lt-PU-FD	2.43 ± 0.02	2.42 ± 0.04	2.43 ± 0.03	2.41 ± 0.05	0.319
Rt-PU-FD	2.43 ± 0.02	2.41 ± 0.04†	2.40 ± 0.04††	2.41 ± 0.05	0.565
Lt-PL-FD	2.34 ± 0.04	2.32 ± 0.06†	2.33 ± 0.04	2.31 ± 0.08†	0.307
Rt-PL-FD	2.36 ± 0.03	2.36 ± 0.06	2.37 ± 0.04	2.34 ± 0.08	0.307
V-FD	2.16 ± 0.05	2.14 ± 0.05	2.14 ± 0.05	2.14 ± 0.06	0.997
Cb-FD	2.51 ± 0.02	2.48 ± 0.04†††	2.48 ± 0.03†††	2.47 ± 0.05††	0.949

SARA: SARA score, Rt: right, Lt: left, Cb: cerebellar, V: vermis, NAA: NAA/Cr ratio, Lt-A-FD: left anterior lobe FD, Rt-A-FD: right anterior lobe FD, Lt-PU-FD: left posterior upper lobe FD, Rt-PU-FD: right posterior upper lobe FD, Lt-PL-FD: left posterior lobe FD, Rt-PL-FD: right posterior lobe FD, V-FD: vermis FD, Cb-FD: FD of the whole cerebellum.
† $p < 0.05$ represents significant difference compared with controls.
†† $p < 0.01$ represents significant difference compared with controls.
††† $p < 0.001$ represents significant difference compared with controls.
* $p < 0.05$ represents significant difference between the two SCA3 subgroups.
** $p < 0.01$ represents significant difference between the two SCA3 subgroups.
*** $p < 0.001$ represents significant difference between the two SCA3 subgroups.
[a] Chi-squared test.

patients than in the controls. These results indicate that SCA3 affects not only the patients' cerebellar function but also the structure of the cerebellar cortex, and they are consistent with the findings in previous reports based on cerebellar NAA measurements (Adanyeguh et al., 2015; Wang et al., 2012), MRI volumetry (Stefanescu et al., 2015) and fMRI (Stefanescu et al., 2015). Moreover, our study findings demonstrate that NAA/Cr and 3D-FD measurements can successfully detect disease involvement in the cerebellar regions.

Table 2
Coefficients of the AO, Duration, CAG repeat length, and AO:CAG in the multivariate linear regression analysis.

Predictors (X_i) Dependent variables (Y)	Intercept	AO	Duration	CAG	AO:CAG
SARA score	−74.222	1.947	1.322***	1.079	−0.027
Rt-Cb-NAA	2.376	−0.028	−0.017**	−0.016	~0
Lt-Cb-NAA	1.733	0.001	−0.014*	−0.006	~0
V-NAA	0.343	0.010	−0.011**	0.008	~0
Lt-A-FD	1.507	0.026	~0	0.010	~0
Rt-A-FD	1.206	0.027	−0.002***	0.013	~0
Lt-PU-FD	1.973**	0.019	−0.001	0.007	~0
Rt-PU-FD	2.035**	0.015	~0	0.006	~0
Lt-PL-FD	2.003	0.014	~0	0.005	~0
Rt-PL-FD	2.026*	0.012	~0	0.005	~0
V-FD	1.886*	0.015	−0.003	0.005	~0
Cb-FD	2.079**	0.013	~0	0.006	~0

Rt: right, Lt: left, Cb: cerebellar, NAA: NAA/Cr ratio, V: vermis, Lt-A-FD: left anterior lobe FD, Rt-A-FD: right anterior lobe FD, Lt-PU-FD: left posterior upper lobe FD, Rt-PU-FD: right posterior upper lobe FD, Lt-PL-FD: left posterior lobe FD, Rt-PL-FD: right posterior lobe FD, V-FD: vermis FD, Cb-FD: FD of the whole cerebellum. CAG: CAG repeat length. AO: age of disease onset. AO:CAG: interaction term of AO and CAG.
* $p < 0.05$ represents significance (FDR corrected).
** $p < 0.01$ represents significance (FDR corrected).
*** $p < 0.001$ represents significance (FDR corrected).

4.2. CAG repeat length is not correlated with SARA score and SARA score/Duration

SARA score was found to be insignificantly correlated with the CAG repeat length of SCA3 patients in this study. A similar result is reported in longitudinal cohort studies (Jacobi et al., 2011; Jacobi et al., 2015). Additionally, SARA score/Duration represents the progression rate of the severity of clinical symptoms. In this study, SARA score/Duration was not correlated with the CAG repeat length of SCA3 patients. Moreover, the average SARA score/Duration values were not different between the SCA3 subgroup with CAG < 74 and that with CAG ≥ 74. This finding is consistent with those in previous reports that have shown that the duration-adjusted International Cooperative Ataxia Rating Scale (ICARS) score (França et al., 2009) and duration-adjusted SARA score (Zhou et al., 2011) were not correlated with the CAG repeat length in SCA3 patients.

These results seem contradictory to those of Klockgether et al., who suggested that a longer CAG repeat length could result in more rapid disease progression in SCA3 patients (Klockgether et al., 1998a). Klockgether et al., classified disease progression into 4 stages depending on the difficulties faced by patients: stage 1, gait difficulties; stage 2, dependence on walking aids; stage 3, wheelchair-bound stage; and stage 4, death. The negative results can be explained by the reason that the progression of the clinical ratings, ICARS and SARA, do not equate to the progression of disease stages.

4.3. CAG repeat length does not significantly affect cerebellar degeneration rate

In this study, we hypothesised that the CAG repeat length may accelerate damage to the cerebellar regions of SCA3 patients. However, our results do not support this hypothesis.

Table 3
Demographic and clinical information of the subjects used in the brain network analysis.

Variables	Control I ($n = 8$)	Control II ($n = 7$)	SCA3	SCA3	p-Value
			CAG < 74 ($n = 8$)	CAG ≥ 74 ($n = 7$)	
Age (year)	50.3 ± 7.9	32.7 ± 7.6†††	50.5 ± 10.6	32.4 ± 5.9	<0.001***
M/F	5/3	6/1	5/3	6/1	0.310[a]
Age of onset (AO) (year)	ND	ND	48.1 ± 11.2	28.7 ± 5.9	0.001**
Duration (year)	ND	ND	2.4 ± 1.2	3.7 ± 1.3	0.051
SARA	ND	ND	6.9 ± 3.8	9.6 ± 7.8	0.396
CAG repeat length	ND	ND	69.0 ± 3.0	76.0 ± 2.4	<0.001***
SARA/Duration (year)	ND	ND	3.2 ± 1.7	2.6 ± 1.8	0.533

No significant difference was observed between the SCA3 subgroups and their corresponding control groups.
** $p < 0.01$ represents the significant difference between the two SCA3 subgroups.
*** $p < 0.001$ represents the significant difference between the two SCA3 subgroups.
††† $p < 0.001$ represents the significant difference between the two control groups.
[a] Chi-squared test.

The multivariate linear regression results show that the CAG repeat length was not a significant determinant of cerebellar NAA/Cr ratios and 3D-FD values. This finding implies that these cerebellar NAA/Cr ratios and 3D-FD values show a similar decline rate in SCA3 patients after the onset of symptoms, regardless of their CAG repeat lengths. Moreover, a nonlinear decline rate of the cerebellar NAA/Cr ratios and 3D-FD values was not observed between the SCA3 subgroup with CAG < 74 and that with CAG ≥ 74. In summary, the CAG repeat length does not exert a significant influence on the degeneration rate of cerebellar function and cerebellar structure.

Similar findings are adequately reported in the literature. Adanyeguh et al. reported that the CAG repeat length was not correlated with the sum of *N*-acetylaspartate and *N*-acetylaspartylglutamate in the cerebellar vermis based on a MRS study (Adanyeguh et al., 2015). In regard to the MRI studies, by using the measure of normalised volume, Klockgether et al. first reported no correlation between the CAG repeat length and the atrophy of cerebellar regions in 11 SCA3 patients (Klockgether et al., 1998b). Subsequently, the same results were found for a higher number of recruited patients (Eichler et al., 2011; Schulz et al., 2010) and in a longitudinal study (Reetz et al., 2013). Recently, a study based on a 7-T MRI modality demonstrated that the CAG repeat

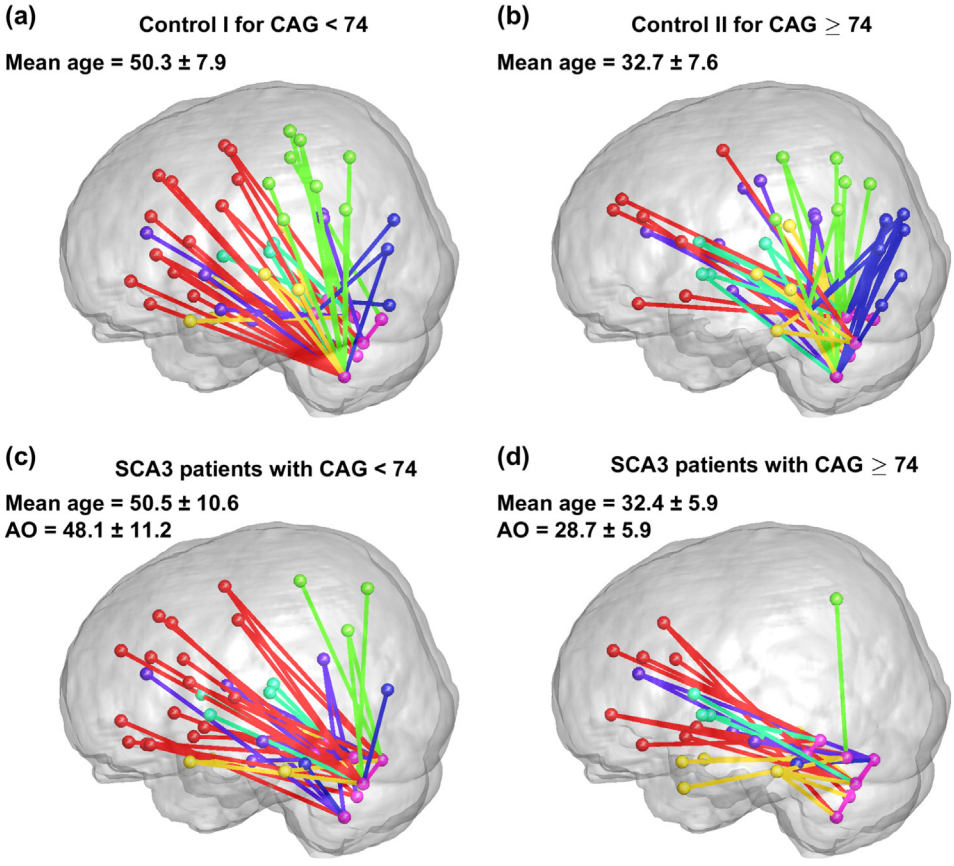

Fig. 6. Cerebellar networks of SCA3 patients and controls. (a) Control I (control group for CAG < 74), (b) Control II (control group for CAG ≥ 74), (c) SCA3 subgroup with CAG < 74, and (d) SCA3 subgroup with CAG ≥ 74. In the diagrams, the nodes in the same brain region are coded in the same colour (red: frontal lobes, green: parietal lobes, blue: occipital lobes, yellow: temporal lobes, purple: limbic system, cyan: subcortical region, and pink: cerebellum). The links connecting the lobes with the cerebellum are colour coded (red: frontal lobes, green: parietal lobes, blue: occipital lobes, yellow: temporal lobes, purple: limbic system, cyan: subcortical region, and pink: cerebellum). (For interpretation of the references to colour in this figure legend, the reader is referred to the web version of this article.)

length was not correlated with the atrophy of the cerebellar cortex or dentate nuclei (Stefanescu et al., 2015). In addition to those neuroimaging reports, a pathoanatomy study also demonstrated that the CAG repeat length was not correlated with the atrophy of the four deep cerebellar nuclei (fastigial nucleus, globose nucleus, emboliform nucleus and dentate nucleus) (Scherzed et al., 2012).

The lack of correlative relationship between the CAG repeat length and the cerebellar degeneration rate is unexpected. So far, the underlying mechanism about how CAG repeat length and other factors control neurodegeneration in SCA3 is unclear. Some studies reported that SCA3 patients could have extracerebellar involvements (Rüb et al., 2008; Rezende et al., 2015; Yamada et al., 2004). Other studies found the degeneration of cerebral regions, basal ganglia, brain stem, spinal cord and white matter in SCA3 is also correlated with SARA score or ICARS score (D'Abreu et al., 2012; Fahl et al., 2015; Kang et al., 2014; Rezende et al., 2015; Schulz et al., 2010). These results indicate that not only the atrophy of cerebellum but also the degeneration of any brain region in the central nervous loop that modulates motor function may arise in ataxia symptoms (Rüb et al., 2008; Schmahmann and Pandya, 2008). Taken together, it is inferred that the earlier onset of ataxia symptoms in the SCA3 patients with a longer CAG repeat length may not be attributed to the more rapid cerebellar degeneration alone. It motivated us to explore whether the SCA3 patients with a longer CAG repeat length may have a different structural covariance network in comparison with those with a shorter CAG repeat length.

4.4. SCA3 patients with longer CAG repeat lengths display dissociation of structural covariance networks between the parietal-occipital lobes and the cerebellum

Our results show that the number of total links in the network and the number of links between the parietal-occipital nodes and the cerebellum were slightly different between Control I and Control II, even though the average age of Control I (50.3 ± 7.9 years) was much higher than that of Control II (32.7 ± 7.6 years). This finding suggests that age does not cause a major difference in the representation of the structural covariance network. However, among the 4 groups, the SCA3 subgroup with CAG ≥ 74 exhibited the fewest total links in the network and the fewest links with the cerebellar regions. Moreover, a disconnection of networks between the parietal-occipital and the cerebellar regions was observed in the SCA3 subgroup with CAG ≥ 74 (mean age = 32.4 ± 5.9 years); by contrast, the disconnection was only mild in the subgroup with CAG < 74 (mean age = 50.5 ± 10.6 years), even though these groups did not exhibit differences in Duration, SARA score, and SARA score/Duration. This result indicates that the SCA3 subgroup with CAG ≥ 74 exhibited dissociated structural covariance networks.

Caution should be exercised when interpreting the results of structural networks constructed according to morphological covariance (e.g., tissue volume, cortical thickness, surface area, concentration, and 3D-FD). The structural covariance may arise from genetic influence, normal development, ageing, mutual trophic influences, or experience-related plasticity (Alexander-Bloch et al., 2013; Evans, 2013). In this study, we did not regress out the effect of age, because of the small sample sizes; the removal of the age effect would result in the disqualification of most links after the thresholding of their *p*-values. Ageing provides a crucial basis of the covariance of 3D-FD values across a group of subjects to preserve an appropriate number of links in the network analysis. Hence, we may assume that the links of the network in Control I and Control II result from morphological changes induced mainly by ageing. Therefore, the decoupling of links in the SCA3 subgroups only reveals that the disease disrupts the structural covariance between paired brain regions through ageing. The cause of the network dissociation between the parietal-occipital regions and the cerebellar regions in the SCA3 patients with CAG ≥ 74 is not yet clearly known. However, SCA3 patients are reported to exhibit widespread disease involvement throughout the brain including parietal-occipital regions (D'Abreu et al., 2012; Rezende et al., 2015; Wang et al., 2015; Yamada et al., 2004). A longer CAG repeat length may result in unbalanced atrophy on the cortex of the parietal-occipital and cerebellar lobes across SCA3 patients, causing the disruption of the structural covariance between parietal-occipital lobes and the cerebellum.

Previous studies have identified changes in the brain network in other genotypes of SCAs caused by mutated CAG expansion. The alteration of the brain network is found to be associated with disease severity and disease duration in SCA1 (Solodkin et al., 2011), cognitive and motor performance (Hernandez-Castillo et al., 2015) and onset of parkinsonism in SCA2 (Wu et al., 2013), visual task performance in SCA6 (Falcon et al., 2015) and CAG repeat length in SCA7 (Hernandez-Castillo et al., 2013). These studies, although mostly based on fMRI, suggest that brain network alteration is associated with clinical variables such as the CAG repeat length, disease severity, disease duration, and task performance in SCAs. The current study is the first to adopt the concept of structural covariance networks to investigate SCAs, and the results demonstrate that the CAG repeat length may affect the cerebellar structural network architecture of SCA3 patients. Taken together, these results demonstrate that these SCAs may be related to 'disconnection syndrome' (Schmahmann and Pandya, 2008).

4.5. Study limitations

This study has several limitations. First, only the cortical atrophy of grey matter was measured by the 3D-FD method in this study. Cerebellar white matter, cerebellar peduncles, and cerebellar deep nuclei, such as dentate nucleus, are not within the scope of this study. This is because the hardware limitation of the imaging modality and the pulse sequence limit the ability to clearly delineate the contours of deep nuclei. Moreover, an automated method to segment these structures is lacking. Second, the sample sizes of the groups included in the brain network analysis might not be sufficient. Third, cross-sectional data of the SCA3 patients were used in this study, and the data were collected after AO, with varied disease duration. Hence, a longitudinal study involving the collection of data before, after, and at the disease onset should be conducted. Lastly, in this study, we divided the SCA3 patients into two subgroups according to a CAG repeat length threshold of 74 (≥74 and <74) to generate two subgroups with balanced sample sizes (22 vs 18). However, different threshold choice might lead to different findings.

5. Conclusions

This study demonstrates that the function and cortical structure of the cerebellum of SCA3 patients are impaired by the disease, which can be detected by MRS NAA/Cr and MRI 3D-FD measures. Nevertheless, we could not find any evidence to support that the CAG repeat length exerts a significant impact on the decline rate of cerebellar function and the atrophy rate of the cerebellar cortex based on NAA/Cr ratios and 3D-FD values. In addition, no correlation was found between the CAG repeat length and SARA score, and between the CAG repeat length and SARA score/Duration in this study. However, a dissociation of the structural covariance network was noted in the SCA3 subgroup with a CAG repeat length ≥ 74, but not in the subgroup with a CAG repeat length < 74. These results suggest that a longer CAG repeat length is not associated with more rapid degeneration of the SARA score or cerebellar function and structure. Nevertheless, a longer CAG repeat length is associated with the disruption of the morphological covariance between paired brain regions. An expansive quantitative network analysis is required to verify this finding in the future.

Acknowledgements

This work was supported by grants from Ministry of Science and Technology (MOST 103-2221-E-010-003-MY3) and Taiwan National Health Research Institutes (NHRI-EX105-10526EI).

Appendix A. Supplementary data

Supplementary data to this article can be found online at http://dx.doi.org/10.1016/j.nicl.2016.11.007.

References

Adanyeguh, I.M., Henry, P.G., Nguyen, T.M., Rinaldi, D., Jauffret, C., Valabregue, R., Emir, U.E., Deelchand, D.K., Brice, A., Eberly, L.E., 2015. In vivo neurometabolic profiling in patients with spinocerebellar ataxia types 1, 2, 3, and 7. Mov. Disord. 30, 662–670.

Alexander-Bloch, A., Giedd, J.N., Bullmore, E., 2013. Imaging structural co-variance between human brain regions. Nat. Rev. Neurosci. 14, 322–336.

Bachelard, H., Badar-Goffer, R., 1993. NMR spectroscopy in neurochemistry. J. Neurochem. 61, 412–419.

Benjamini, Y., Hochberg, Y., 1995. Controlling the false discovery rate: a practical and powerful approach to multiple testing. J. R. Stat. Soc. Ser. B Methodol. 289–300.

Braun, U., Muldoon, S.F., Bassett, D.S., 2009. On human brain networks in health and disease. eLS.

D'Abreu, A., Franca Jr., M.C., Yasuda, C.L., Campos, B.A., Lopes-Cendes, I., Cendes, F., 2012. Neocortical atrophy in Machado-Joseph disease: a longitudinal neuroimaging study. J. Neuroimaging 22, 285–291.

do Carmo Costa, M., Paulson, H.L., 2012. Toward understanding Machado–Joseph disease. Prog. Neurobiol. 97, 239–257.

Durr, A., Stevanin, G., Cancel, G., Duyckaerts, C., Abbas, N., Didierjean, O., Chneiweiss, H., Benomar, A., Lyon-Caen, O., Julien, J., 1996. Spinocerebellar ataxia 3 and Machado-Joseph disease: clinical, molecular, and neuropathological features. Ann. Neurol. 39, 490–499.

Eichler, L., Bellenberg, B., Hahn, H., Köster, O., Schöls, L., Lukas, C., 2011. Quantitative assessment of brain stem and cerebellar atrophy in spinocerebellar ataxia types 3 and 6: impact on clinical status. Am. J. Neuroradiol. 32, 890–897.

Evans, A.C., 2013. Networks of anatomical covariance. NeuroImage 80, 489–504.

Fahl, C.N., Branco, L.M.T., Bergo, F.P., D'Abreu, A., Lopes-Cendes, I., França Jr., M.C., 2015. Spinal cord damage in Machado-Joseph disease. Cerebellum 14, 128–132.

Falcon, M., Gomez, C., Chen, E., Shereen, A., Solodkin, A., 2015. Early cerebellar network shifting in spinocerebellar ataxia type 6. Cereb. Cortex, bhv154.

França, M.C., D'Abreu, A., Nucci, A., Cendes, F., Lopes-Cendes, I., 2009. Progression of ataxia in patients with Machado-Joseph disease. Mov. Disord. 24, 1387–1390.

Friston, K.J., 1994. Functional and effective connectivity in neuroimaging: a synthesis. Hum. Brain Mapp. 2, 56–78.

Gong, G., He, Y., Chen, Z.J., Evans, A.C., 2012. Convergence and divergence of thickness correlations with diffusion connections across the human cerebral cortex. NeuroImage 59, 1239–1248.

Guimaraes, R.P., D'Abreu, A., Yasuda, C.L., França, M.C., Silva, B.H., Cappabianco, F.A., Bergo, F.P., Lopes-Cendes, I.T., Cendes, F., 2013. A multimodal evaluation of microstructural white matter damage in spinocerebellar ataxia type 3. Mov. Disord. 28, 1125–1132.

Ha, T.H., Yoon, U., Lee, K.J., Shin, Y.W., Lee, J.-M., Kim, I.Y., Ha, K.S., Kim, S.I., Kwon, J.S., 2005. Fractal dimension of cerebral cortical surface in schizophrenia and obsessive–compulsive disorder. Neurosci. Lett. 384, 172–176.

Hernandez-Castillo, C.R., Alcauter, S., Galvez, V., Barrios, F.A., Yescas, P., Ochoa, A., Garcia, L., Diaz, R., Gao, W., Fernandez-Ruiz, J., 2013. Disruption of visual and motor connectivity in spinocerebellar ataxia type 7. Mov. Disord. 28, 1708–1716.

Hernandez-Castillo, C.R., Galvez, V., Mercadillo, R.E., Díaz, R., Yescas, P., Martinez, L., Ochoa, A., Velazquez-Perez, L., Fernandez-Ruiz, J., 2015. Functional connectivity changes related to cognitive and motor performance in spinocerebellar ataxia type 2. Mov. Disord. 30, 1391–1399.

Jacobi, H., Bauer, P., Giunti, P., Labrum, R., Sweeney, M., Charles, P., Dürr, A., Marelli, C., Globas, C., Linnemann, C., 2011. The natural history of spinocerebellar ataxia type 1, 2, 3, and 6: a 2-year follow-up study. Neurology 77, 1035–1041.

Jacobi, H., du Montcel, S.T., Bauer, P., Giunti, P., Cook, A., Labrum, R., Parkinson, M.H., Durr, A., Brice, A., Charles, P., 2015. Long-term disease progression in spinocerebellar ataxia types 1, 2, 3, and 6: a longitudinal cohort study. Lancet Neurol. 14, 1101–1108.

Jardim, L.B., Pereira, M.L., Silveira, I., Ferro, A., Sequeiros, J., Giugliani, R., 2001. Neurologic findings in Machado-Joseph disease: relation with disease duration, subtypes, and (CAG) n. Arch. Neurol. 58, 899–904.

Kang, J.-S., Klein, J., Baudrexel, S., Deichmann, R., Nolte, D., Hilker, R., 2014. White matter damage is related to ataxia severity in SCA3. J. Neurol. 261, 291–299.

Kawaguchi, Y., Okamoto, T., Taniwakiz, M., Aizawa, M., 1994. CAG expansions in a novel gene for Machado-Joseph disease at. Nat. Genet. 8, 221–228.

King, R.D., Brown, B., Hwang, M., Jeon, T., George, A.T., Initiative, A.S.D.N., 2010. Fractal dimension analysis of the cortical ribbon in mild Alzheimer's disease. NeuroImage 53, 471–479.

Klockgether, T., Lüdtke, R., Kramer, B., Abele, M., Bürk, K., Schöls, L., Riess, O., Laccone, F., Boesch, S., Lopes-Cendes, I., 1998a. The natural history of degenerative ataxia: a retrospective study in 466 patients. Brain 121, 589–600.

Klockgether, T., Skalej, M., Wedekind, D., Luft, A., Welte, D., Schulz, J., Abele, M., Bürk, K., Laccone, F., Brice, A., 1998b. Autosomal dominant cerebellar ataxia type I. MRI-based volumetry of posterior fossa structures and basal ganglia in spinocerebellar ataxia types 1, 2 and 3. Brain 121, 1687–1693.

Koeppen, A.H., 2005. The pathogenesis of spinocerebellar ataxia. Cerebellum 4, 62–73.

Lerch, J.P., Worsley, K., Shaw, W.P., Greenstein, D.K., Lenroot, R.K., Giedd, J., Evans, A.C., 2006. Mapping anatomical correlations across cerebral cortex (MACACC) using cortical thickness from MRI. NeuroImage 31, 993–1003.

Lirng, J.-F., Wang, P.-S., Chen, H.-C., Soong, B.-W., Guo, W.Y., Wu, H.-M., Chang, C.-Y., 2012. Differences between spinocerebellar ataxias and multiple system atrophy-cerebellar type on proton magnetic resonance spectroscopy. PLoS One 7, e47925.

Maciel, P., Gaspar, C., DeStefano, A.L., Silveira, I., Coutinho, P., Radvany, J., Dawson, D.M., Sudarsky, L., Guimarães, J., Loureiro, J.E., 1995. Correlation between CAG repeat length and clinical features in Machado-Joseph disease. Am. J. Hum. Genet. 57, 54.

Onodera, O., Idezuka, J., Igarashi, S., Takiyama, Y., Endo, K., Takano, H., Oyake, M., Tanaka, H., Inuzuka, T., Hayashi, T., 1998. Progressive atrophy of cerebellum and brainstem as a function of age and the size of the expanded CAG repeats in the MJD1 gene in Machado-Joseph disease. Ann. Neurol. 43, 288–296.

Pedroso, J.L., França, M.C., Braga-Neto, P., D'Abreu, A., Saraiva-Pereira, M.L., Saute, J.A., Teive, H.A., Caramelli, P., Jardim, L.B., Lopes-Cendes, I., 2013. Nonmotor and extracerebellar features in Machado-Joseph disease: a review. Mov. Disord. 28, 1200–1208.

Reetz, K., Costa, A.S., Mirzazade, S., Lehmann, A., Juzek, A., Rakowicz, M., Boguslawska, R., Schöls, L., Linnemann, C., Mariotti, C., 2013. Genotype-specific patterns of atrophy progression are more sensitive than clinical decline in SCA1, SCA3 and SCA6. Brain 136, 905–917.

Rezende, T., D'Abreu, A., Guimarães, R., Lopes, T., Lopes-Cendes, I., Cendes, F., Castellano, G., França, M., 2015. Cerebral cortex involvement in Machado–Joseph disease. Eur. J. Neurol. 22, 277-e224.

Rüb, U., Brunt, E.R., Deller, T., 2008. New insights into the pathoanatomy of spinocerebellar ataxia type 3 (Machado–Joseph disease). Curr. Opin. Neurol. 21, 111–116.

Rubinov, M., Sporns, O., 2010. Complex network measures of brain connectivity: uses and interpretations. NeuroImage 52, 1059–1069.

Sandu, A.-L., Rasmussen, I.-A., Lundervold, A., Kreuder, F., Neckelmann, G., Hugdahl, K., Specht, K., 2008. Fractal dimension analysis of MR images reveals grey matter structure irregularities in schizophrenia. Comput. Med. Imaging Graph. 32, 150–158.

Scherzed, W., Brunt, E., Heinsen, H., de Vos, R., Seidel, K., Bürk, K., Schöls, L., Auburger, G., Del Turco, D., Deller, T., 2012. Pathoanatomy of cerebellar degeneration in spinocerebellar ataxia type 2 (SCA2) and type 3 (SCA3). Cerebellum 11, 749–760.

Schmahmann, J.D., Pandya, D.N., 2008. Disconnection syndromes of basal ganglia, thalamus, and cerebrocerebellar systems. Cortex 44, 1037–1066.

Schmitz-Hübsch, T., Du Montcel, S.T., Baliko, L., Berciano, J., Boesch, S., Depondt, C., Giunti, P., Globas, C., Infante, J., Kang, J.-S., 2006. Scale for the assessment and rating of ataxia development of a new clinical scale. Neurology 66, 1717–1720.

Schulz, J.B., Borkert, J., Wolf, S., Schmitz-Hübsch, T., Rakowicz, M., Mariotti, C., Schoels, L., Timmann, D., van de Warrenburg, B., Dürr, A., 2010. Visualization, quantification and correlation of brain atrophy with clinical symptoms in spinocerebellar ataxia types 1, 3 and 6. NeuroImage 49, 158–168.

Solodkin, A., Peri, E., Chen, E.E., Ben-Jacob, E., Gomez, C.M., 2011. Loss of intrinsic organization of cerebellar networks in spinocerebellar ataxia type 1: correlates with disease severity and duration. Cerebellum 10, 218–232.

Soong, B.-W., Lu, Y.-C., Choo, K.-B., Lee, H.-Y., 2001. Frequency analysis of autosomal dominant cerebellar ataxias in Taiwanese patients and clinical and molecular characterization of spinocerebellar ataxia type 6. Arch. Neurol. 58, 1105–1109.

Stefanescu, M.R., Dohnalek, M., Maderwald, S., Thürling, M., Minnerop, M., Beck, A., Schlamann, M., Diedrichsen, J., Ladd, M.E., Timmann, D., 2015. Structural and functional MRI abnormalities of cerebellar cortex and nuclei in SCA3, SCA6 and Friedreich's ataxia. Brain 138, 1182–1197.

Takiyama, Y., Oyanagi, S., Kawashima, S., Sakamoto, H., Saito, K., Yoshida, M., Tsuji, S., Mizuno, Y., Nishizawa, M., 1994. A clinical and pathologic study of a large Japanese family with Machado-Joseph disease tightly linked to the DNA markers on chromosome 14q. Neurology 44, 1302.

Thompson, P.M., Lee, A.D., Dutton, R.A., Geaga, J.A., Hayashi, K.M., Eckert, M.A., Bellugi, U., Galaburda, A.M., Korenberg, J.R., Mills, D.L., 2005. Abnormal cortical complexity and thickness profiles mapped in Williams syndrome. J. Neurosci. 25, 4146–4158.

Wang, P.-S., Chen, H.-C., Wu, H.-M., Lirng, J.-F., Wu, Y.-T., Soong, B.-W., 2012. Association between proton magnetic resonance spectroscopy measurements and CAG repeat number in patients with spinocerebellar ataxias 2, 3, or 6. PLoS One 7, e47479.

Wang, Z., Dai, Z., Gong, G., Zhou, C., He, Y., 2014. Understanding structural-functional relationships in the human brain a large-scale network perspective. Neuroscientist 1073858414537560.

Wang, T.-Y., Jao, C.-W., Soong, B.-W., Wu, H.-M., Shyu, K.-K., Wang, P.-S., Wu, Y.-T., 2015. Change in the cortical complexity of spinocerebellar ataxia type 3 appears earlier than clinical symptoms. PLoS One 10.

Wang, P.-S., Liu, R.-S., Yang, B.-H., Soong, B.-W., 2007. Regional patterns of cerebral glucose metabolism in spinocerebellar ataxia type 2, 3 and 6. J. Neurol. 254, 838–845.

Wu, Y.-T., Shyu, K.-K., Jao, C.-W., Wang, Z.-Y., Soong, B.-W., Wu, H.-M., Wang, P.-S., 2010. Fractal dimension analysis for quantifying cerebellar morphological change of multiple system atrophy of the cerebellar type (MSA-C). NeuroImage 49, 539–551.

Wu, T., Wang, C., Wang, J., Hallett, M., Zang, Y., Chan, P., 2013. Preclinical and clinical neural network changes in SCA2 Parkinsonism. Parkinsonism Relat. Disord. 19, 158–164.

Yamada, M., Tan, C.F., Inenaga, C., Tsuji, S., Takahashi, H., 2004. Sharing of polyglutamine localization by the neuronal nucleus and cytoplasm in CAG-repeat diseases. Neuropathol. Appl. Neurobiol. 30, 665–675.

Zhou, J., Lei, L., Liao, X., Wang, J., Jiang, H., Tang, B., Shen, L., 2011. Related factors of ICARS and SARA scores on spinocerebellar ataxia type 3/Machado-Joseph disease. Zhong Nan Da Xue Xue Bao Yi Xue Ban 36, 498–503.